Veterinary Microbiology 320 (2026) 111095

Contents lists available at ScienceDirect

Veterinary Microbiology

journal homepage: www.elsevier.com/locate/vetmic

Prenatal APPV infection delays cerebellar myelination and alters gene expression dynamics during recovery from congenital tremor in pigs

Anna Bergfeldt *, Michael A. Tranulis, Randi Sørby

Department of Preclinical Sciences and Pathology, Faculty of Veterinary Medicine, Norwegian University of Life Sciences, PO box 5003, Ås 1432, Norway

ARTICLE INFO

Keywords:
Atypical porcine pestivirus
Congenital tremor type A-II
Pathogenesis
Myelination
Transcriptomics
Immunohistochemistry

ABSTRACT

Atypical porcine pestivirus (APPV) causes congenital tremor (CT) type A-II in piglets, a globally distributed neurological condition, yet its impact on central nervous system (CNS) development and recovery remains poorly understood. This longitudinal case-control study investigated APPV-induced alterations in cerebellar and cerebral cellular processes during clinical disease and recovery by integrating transcriptomic profiling with immunohistochemistry (IHC) in CT pigs at three ages (newborn, 3-week-old, 4–5 months) compared to controls. Group-level transcriptional patterns were assessed using cerebellar RNA-sequencing, complemented by individual-level RNA-seq of cerebral white matter. Prenatal APPV infection was associated with delayed expression of myelin-associated genes, most pronounced in the cerebellum. Despite early deficits, oligodendrocyte populations were preserved and recovered pigs showed upregulation of myelination-related genes, indicating compensatory repair. Early disease stages lacked overt inflammation, with gene expression findings suggesting immune modulation consistent with known pestiviral interferon antagonist activity, while astrocyte hypertrophy in newborns and microglial aggregates in recovered pigs revealed dynamic glial remodelling. These findings provide novel insights into APPV-induced myelination delay and highlight glial plasticity as a key factor in CNS repair following developmental viral disruption. Further research is needed to clarify primary in utero responses to APPV infection underlying the congenital hypomyelination.

1. Background

Congenital tremor (CT) type A-II is a neurological disease in pigs that compromises welfare and health. CT A-II presents as intentional tremors of varying severity (Dall Agnol et al., 2020), with outbreaks showing high morbidity and slightly increased pre-weaning mortality, mainly due to trauma and secondary infections from reduced motility and suckling (Arruda et al., 2016; Stenberg et al., 2020). Survivors typically recover by three months of age (Arruda et al., 2016; de Groof et al., 2016; Schwarz et al., 2017).

Atypical porcine pestivirus (APPV; also designated APPeV), a positive-sense RNA virus in the genus Pestivirus (*Flaviviridae*) discovered in 2015 is now recognised as the primary cause for CT A-II (Arruda et al., 2016; de Groof et al., 2016; Hause et al., 2015). Clinical disease follows vertical transmission while horizontal infection is transient and subclinical (Cagatay et al., 2019). In affected newborns, mild hypomyelination and variable myelin vacuolisation occur in the central nervous system (CNS), particularly in the cerebellum and spinal cord (Schwarz et al., 2017; Postel et al., 2016), impairing nerve conduction and causing the tremors.

APPV exhibits CNS tropism, especially in the cerebellum, where it can persist at high levels in both newborns and recovered pigs (Liu et al., 2019; Buckley et al., 2021). At the cellular level, APPV localises to neurons in the cerebellar internal granular layer and molecular layers, but not Purkinje cells (Buckley et al., 2021), and has also been detected in white matter nerve fibres (Liu et al., 2019).

Myelination is a complex process, vulnerable to disruption through direct oligodendrocyte dysfunction or indirect effects mediated by microglia, astrocytes or neuronal interactions. Such disturbances can lead to lesions, as observed in CT A-II. Despite glial cells' critical role in CNS development, few studies have examined APPV's impact on glial activity. Existing work reports similar OLIG2 + (Oligodendrocyte transcription factor 2) oligodendrocyte lineage cells densities in CT pigs and controls (Schwarz et al., 2017), and increased GFAP + (Glial fibrillary acidic protein) astrocyte proliferation (astrogliosis) in APPV-positive piglets (Possatti et al., 2018). Both studies focused on newborns, leaving recovery mechanisms largely uncharacterised.

Both vertical and horizontal transmission can lead to prolonged

* Corresponding author.
E-mail addresses: anbe@vetinst.no (A. Bergfeldt), michael.tranulis@nmbu.no (M.A. Tranulis), randi.sorby@nmbu.no (R. Sørby).

https://doi.org/10.1016/j.vetmic.2026.111095
Received 21 February 2026; Received in revised form 24 April 2026; Accepted 26 May 2026
Available online 27 May 2026

infection, likely due to interferon suppression (Cagatay et al., 2019). Mild antiviral cytokine responses have been observed in newborns (Stenberg et al., 2022), but immune dynamics during recovery remain unclear. Whether persistent infection (virus positive and antibody negative animals) occurs in APPV infection as for classical pestiviruses, is unknown.

CT A-II is significant for pig production due to its endemic nature and welfare impact. The pathogenesis of APPV infection with its postnatal effects on CNS development and glial cell behaviour during recovery is poorly understood. This study aimed to address these gaps by (i) characterising APPV-associated processes in the cerebellum and cerebral white matter, and their progression during recovery (ii) identifying candidate biomarkers from transcriptomic analyses for immunohistochemical evaluation; and (iii) correlating immunohistochemical findings with transcriptomics profiles to clarify glial cell roles during CNS recovery.

2. Material and methods

2.1. Ethical considerations

The study was approved by the Norwegian Food Safety Authority (FOTS ID: 25780) and conducted in accordance with Norwegian animal welfare legislation.

2.2. Study design and sampling

This study was part of a larger Norwegian field investigation (2021–2022) that previously reported longitudinal clinical and pathological findings in CT A-II (Aae et al., 2025; Bergfeldt et al., 2025).

In this descriptive case-control design, samples were collected from herds with CT outbreaks and from a control farm. Five pigs were sampled from each of three age groups: newborns (2–4 days), 3-week-olds, and 4-to−5-month-olds. All affected newborns exhibited severe tremors, which diminished by three weeks and were nearly absent at the final sampling (Aae et al., 2025). Clinical, necropsy, and histopathological examinations revealed no concurrent disease or signs of other conditions that could confound CT pathogenesis (Aae et al., 2025; Bergfeldt et al., 2025). Based on the absence of clinical or histopathological findings suggestive of co-existing disease, and the official status as disease-free from viral pathogens known to represent relevant differential diagnoses for tremor disorders in piglets (e.g. classical swine fever virus and porcine reproductive and respiratory syndrome virus) in Norway, no additional diagnostic testing was performed beyond APPV detection. All CT-affected pigs included in the present study were APPV-positive in serum during the neonatal period (2–4 days of age). Longitudinal assessment of viremia and APPV-specific antibody responses was performed in a separate cohort within the same field study and is reported elsewhere.

Brain tissue was collected within 20 min post-euthanasia. Samples for RNA sequencing were dissected into ~20 mg pieces, placed in RNA*later* (Thermo Fisher, Massachusetts, United States) for 24 hr at room temperature, and stored at −80 °C. Brain samples for histology were fixed in 10% neutral-buffered formalin for 10–14 days.

Morphological studies revealed variable white matter vacuolisation, mild myelin disruption and cerebellar hypomyelination in CT affected pigs. All CT-affected piglets were APPV-positive in CNS samples by RT-qPCR, with highest levels in the cerebellum, whereas controls were negative. RNA analyses were restricted to CNS tissues, as systemic distribution of APPV has been demonstrated previously (Postel et al., 2016; Liu et al., 2019), and no histological lesions were observed outside the CNS. Cerebellar viral load peaked at three weeks and remained elevated at 4–5 months, while cerebral viral load was consistently lower across all ages (Bergfeldt et al., 2025).

Based on these findings, cerebellum and cerebral white matter were selected for transcriptomic analysis. Two phases were conducted: (i) pooled cerebellar samples (grey and white matter) to identify robust, group-level transcriptional patterns and biological processes associated with APPV infection across disease stages, and (ii) individual cerebral samples (white matter only) to enable higher-resolution analysis of white matter-specific changes at the individual level.

2.3. RNA extraction and sample preparation

For cerebellar RNA sequencing, total RNA was isolated from ~20 mg of tissue from the lateral hemisphere using the RNeasy protocol for lipid-rich tissue (Qiagen, Gaithersburg, MD, USA) on a Qiagen QIAsymphony SP instrument, following manufacturer instructions. RNA concentration was measured with a Qubit 2.0 Fluorometer with the Qubit RNA HS Assay Kit (Thermo Fisher Scientific, Paisley, UK), and quality assessed using an Epoch Microplate Spectrophotometer (BioTek, Winooski, VT, USA).

Samples from each pig were normalised to 45 ng/µl and pooled by combining 4 µl from all five pigs per group, yielding six pooled samples. RNA integrity (RIN $>$ 6.5) was confirmed using a TapeStation (Agilent, Santa Clara, CA, USA).

To complement pooled cerebellar data, a second sequencing round targeted white matter at individual level. Due to limited cerebellar white matter, RNA was extracted from cerebral tissue, primarily large tracts at the thalamic level (e.g. internal capsule). For three CT newborns, white matter from more rostral part of internal capsule (at motor cortex level) was used. RNA was isolated from 20 to 25 mg tissue using the Maxwell HT simplyRNA kit (Promega, Madison, WI, USA) on a Biomek 4000 Laboratory Automation Workstation (Beckman Coulter, Brea, CA, USA). Quality control followed the same protocol as for cerebellar samples.

Pooled cerebellar samples were shipped on dry ice to Novogene, Cambridge, UK, and individual cerebral samples were shipped Novogene, Munich, Germany. Library preparation, sequencing and the bioinformatics pipeline were identical for both rounds.

2.4. Library preparation and RNA sequencing

After RNA quality assessment, mRNA was enriched using oligo(dT) magnetic beads targeting poly-A tails. The isolated mRNA was fragmented and reverse-transcribed into first-strand cDNA with random primers, followed by second-strand synthesis incorporating dUTP for strand specificity.

Libraries were prepared through end-repair, A-tailing, and ligation of indexed adapters, then PCR-amplified by PCR and purified. Quality and concentration were verified using a Qubit fluorometer (Thermo Fisher Scientific, Paisley, UK) and qPCR, and fragment size distribution assessed with an Agilent Bioanalyzer (Agilent Technologies, Santa Clara, CA, USA). Sequencing was performed on an Illumina NovaSeq 6000 platform using 150 bp paired-end reads.

Data analysis was conducted by Novogene using a standard pipeline. Raw reads (FASTQ format) were quality-checked and aligned to the *Sus scrofa* genome (NCBI: txid415978) with HISAT2 (v.2.0.5). Post-filtering, clean reads averaged 99% for cerebellum and 93% for cerebrum samples, with Q30 scores $>$ 92% and GC content of 53.5% and 51.9%, respectively. Unique alignment rates were 93.4% and 92, 7%. Detailed quality metrics are provided in Supplementary Tables S1-S2.

Gene expression levels were normalised for transcript length and sequencing depth and reported as FPKM (Fragments Per Kilobase of transcript per Million mapped reads).

2.5. Analysis of differentially expressed genes (DEGs)

Differential gene expression analysis was performed using DESeq2. Genes with a $\log_2$(fold change) ≥ 1 ($\geq$ twofold difference) and a false discovery rate (FDR) of $q < 0.05$ were considered differentially expressed for both cerebellar and cerebral samples across all age groups. Heatmaps were generated in R (v.3.0.3) using ggplot2 and pheatmap to

visualise clustering of DEGs and sample expression patterns.

2.6. Functional enrichment analysis

Gene ontology (GO) and pathway enrichment analysis were conducted on DEG lists to assess APPV's functional impact in cerebellum and cerebrum. Up- and down-regulated genes for each age group were analysed using DAVID (Database for Annotation, Visualization and Integrated Discovery), with the *Sus scrofa* genome as background. GO enrichment focused on Biological Process (BP) terms using the GOTERM_BP_ALL category, and KEGG (Kyoto Encyclopedia of Genes and Genomes) pathways were also assessed. Enrichment was considered significant at FDR $q < 0.05$. All DEGs were successfully matched to the database.

Evaluation of enriched biological processes focused primarily on those with a clear connection to glial cell development, glial function, or immune responses.

2.7. Immunohistochemistry (IHC) targeting glial proteins

IHC was performed on cerebellar tissue to localise glial cell proteins and complement RNA-seq findings. Target antigens, antibodies and characteristics are summarised in Table 1.

Frontal sections from the right lateral cerebellar hemisphere (approx. P14.00 mm, based on a pig brain stereotaxic atlas (Felix et al., 1999) were used for all pigs. Negative controls included sections incubated without primary antibody.

Formalin-fixed, paraffin-embedded slides were deparaffinated in xylene, rehydrated through graded ethanol, and rinsed in distilled water. Antigen retrieval was performed as follows: proteolytic digestion for IBA1 (Ionized calcium-binding adaptor molecule 1) (trypsin buffer, pH 8.0, 37°C, 40 min); heat-induced retrieval for OLIG2 and MBP (Myelin basic protein) (Tris-EDTA, pH 9.0, 110°C, 10 min); none for GFAP.

For all rabbit-derived antibodies, the MACH1 Universal HRP-Polymer Detection Kit (Biocare Medical, LLC, Concord, CA, USA) was used for peroxidase inhibition, background blocking, and HRP-polymer binding, according to the manufacturer's instructions. Primary antibodies were incubated for 30 min.

For MBP, inhibition was performed in 3% H_2O_2/methanol (10 min), followed by blocking in rabbit serum (1:50 in PBS, 1 h). Slides were incubated overnight at 4°C with primary antibody diluted in 1% BSA/TBS, then with Rabbit Anti-Rat (HRP) (Article No: LS-C346721–1, Nordic BioSite), diluted 1:50 in rabbit serum (1:50 in PBS), for 1.5 h. Signal amplification used the ABC Elite Kit (Vectastain, Vector laboratories, Burlingame, CA, USA).

Immunolabeling was visualised with AEC Romulin Chromogen Kit (BioCare medical, LCC) according to instructions by the manufacturer. PBS washes were performed between steps (except after blocking). Unless specified, incubations were at room temperature. Slides were counterstained with hematoxylin, dehydrated, cleared in xylene and coverslipped.

2.8. Quantitative IHC analysis in Qupath

Semi-automatic evaluation of IHC slides was performed using QuPath (v.0.5.1) (Bankhead et al., 2017). Slides were scanned on a Philips IntelliSite Ultra-fast Scanner, saved as TIFF files and assigned unique IDs to maintain unbiased evaluation. IDs were later linked to sample identifiers.

Separate QuPath projects were created for each antibody to ensure consistent analysis. Images were set to "Brightfield H-DAB" and staining vectors were calibrated from representative images to separate hematoxylin and AEC components. Standardised stain settings were applied across all images.

Four rectangular annotations (0.67 mm^2, 1000 ×750 μm) were placed along the lateral periphery of unbranched white matter, avoiding artifacts and ensuring uniform stain intensity. Immunolabeling was quantified as mean percentage of positive area per mm^2 or number of positive cells per mm^2.

For OLIG2, positive cell detection was used to count OLIG2 + nuclei and calculate histochemistry scores (H-scores) based on intensity thresholds. For cytoplasmic markers (GFAP, IBA1 and MBP), AEC-stained pixels were detected using threshold commands on the DAB channel to determine labelled areas. Intensity thresholds (1 +, 2 +, 3 +) were analysed for MBP and GFAP (newborn group) due to observed variability. QuPath commands and threshold settings are summarised in Supplementary Table S3.

Additionally, IBA1 analysis included microglial aggregates (clusters of ≥ 3 microglia within unbranched white matter) to account for distribution differences observed during evaluation.

2.9. Statistical analysis

Mean gene expression was calculated from counts normalised for sequencing dept, with relative expression presented using control newborns as reference. Group differences were assessed in Jamovi (v.2.3.18), using the Mann-Whitney *U* test. Figures illustrating DEGs and quantitative IHC results were created in BioRender.com.

2.10. Data availability

The raw RNA-seq data generated in this study have been deposited in the European Nucleotide Archive (ENA) at EMBL-EBI under the accession number PRJEB108559.

All processed data, including differential expression tables, GO/KEGG enrichment results, are available as Supplementary files.

3. Results

3.1. Age- and region-dependent differences in differential gene expression (DEG)

A total of 1103 differently expressed protein-coding genes (DEGs) were identified in the cerebellum and 426 in the cerebrum across the three age groups.

In the cerebellum, DEG numbers increased with age (Fig. 1**a**): newborns had 68 DEGs (22 upregulated, 46 downregulated), 3-week-olds had 371 (150 upregulated, 221 downregulated), and 4–5-month-olds had 659 (506 upregulated, 153 downregulated). In contrast, the cerebrum showed the highest DEG count in newborns (n = 373; 309 upregulated, 64 downregulated), dropping to 50 in 3-week-olds and 40 in

Table 1
Antibodies used for immunohistochemical detection of glial markers.

Target Antigen	Source and cat.nr.	Raised in	Dilution	Target cells	Localisation
GFAP	Dako Z033429–2	Rabbit	1:1000	Astrocytes	Cytoplasm, filament
IBA1	FUJIFILM Wako, 019–19741	Rabbit	1:500	Microglia	Cytoplasm
OLIG2	Sigma-Aldrich. AB9610.	Rabbit	1:200	Oligodendrocytes, all stages	Nucleus
MBP	Abcam, cat.nr. ab7349.	Rat	1:100	Mature oligodendrocytes	Myelin sheath

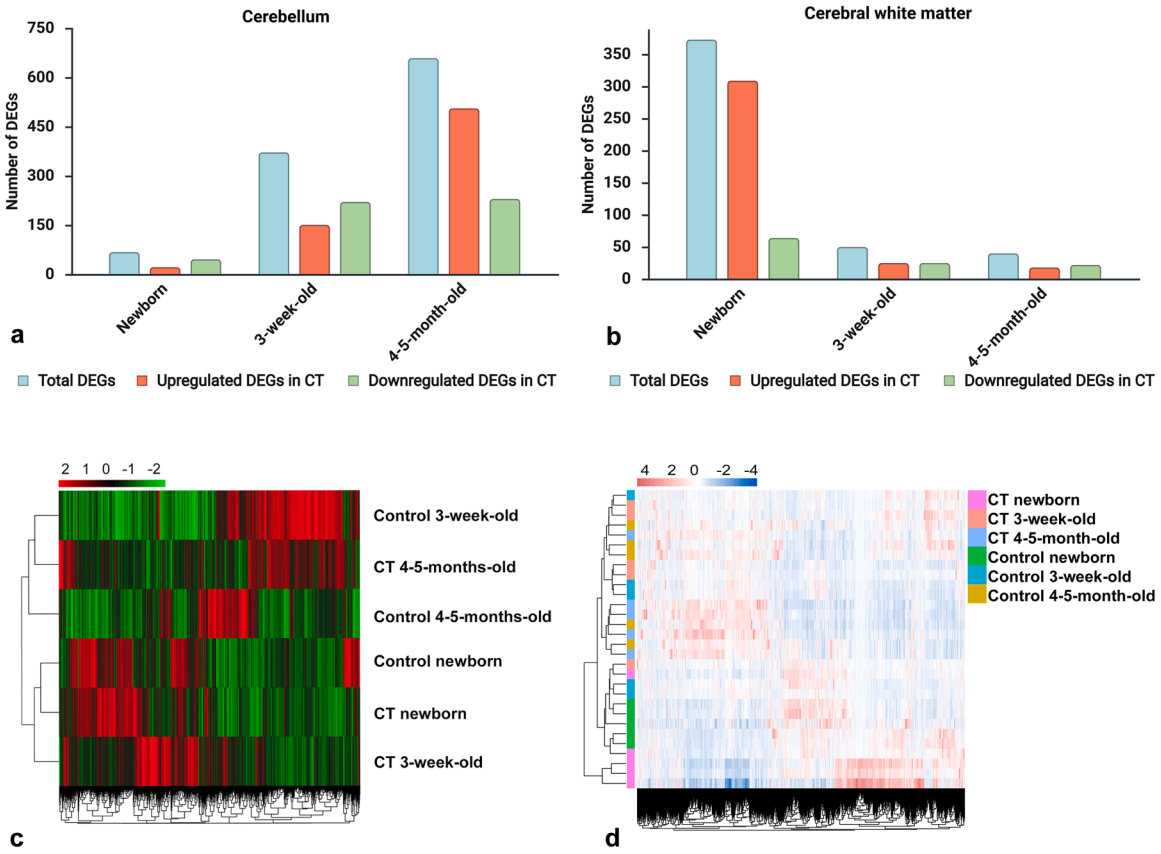

Fig. 1. Longitudinal analysis of differentially expressed genes (DEGs) in the CNS of pigs with congenital tremor (CT). (a) DEG counts in pooled cerebellar samples from CT pigs versus age-matched controls across three age groups. (b) DEG counts in individual cerebral white matter samples. (c) Heatmap of pooled cerebellar samples showing clustering of genes (columns) and samples (rows) by expression patterns: red indicates high expression, green low. (d) Heatmap of individual cerebral white matter samples highlighting distinct expression difference between white matter from caudal and rostral internal capsule in cerebrum in CT newborns (three bottom rows), rendering newborn DEG results from rostral cerebrum unreliable for further analysis. In this heatmap, red still indicates high expression, while blue indicates low.

4–5-month-olds (Fig. 1**b**).

Heatmap clustering revealed that cerebellar expression patterns were most similar between CT newborns and controls, and between 4 and 5-month-old CT pigs and 3-week-old controls (Fig. 1**c**). Interestingly, 3-weeks old CT pigs resembled newborn controls more than their age-matched controls.

In the cerebrum, heatmap analysis showed that the three CT newborn samples from the more rostral part of internal capsule differed markedly from samples taken more caudally (at the thalamic level) (Fig. 1**d**). These differences were supported by additional analyses (principal component analysis, Venn-diagrams, and gene counts). To avoid confounding, these three samples were excluded from further analysis. Apart from this, heatmaps for cerebral white matter showed less distinct group differences between CT pigs and controls, with 4–5-month-old CT pigs displaying the greatest intra-group similarity.

Detailed DEG lists for all age groups and tissues are provided in Supplementary Tables S4–S9.

3.2. *Biological processes enrichment increases with age in CT pigs*

In 3-week-old CT pigs, 92 biological processes were upregulated and 30 were downregulated, while in 4–5-months-old CT pigs 256 processes were upregulated and 3 were downregulated. In newborns, however, no significantly overrepresented processes were detected, and no clear upstream regulators emerged. Detailed lists of enriched biological processes are provided in Supplementary tables S10 to S13.

For the cerebrum, enrichment analysis of newborn samples yielded significant terms, but these were excluded due to tissue heterogeneity, and no enriched processes were found in the older cerebral groups.

3.3. *Myelination delay in the cerebellum of recovering CT pigs*

GO enrichment analysis of downregulated genes in 3-week-old CT pigs showed overrepresentation of myelination, oligodendrocyte development, and differentiation terms, many of which were upregulated in the 4–5-month-old CT pigs (Table 2**),** consistent with a delay in cerebellar myelination.

Key myelination DEGs at both three weeks and 4–5 months included genes coding for structural myelin proteins, such as *MBP* and *PLP1* (Proteolipid protein 1), adhesion/axon-glia interaction proteins, such as *MAG* (Myelin-associated glycoprotein) and *MAL* (Myelin and lymphocyte protein), and proteins supporting non-compact myelin, such as *CNP* (2'3'-Cyclic nucleotide 3'-Phosphodiesterase). Transcriptional regulators spanned pan-stage factors, such as *OLIG2* and *SOX10* (SRY-box transcription factor 10); early regulators, such as *NKX6–2* (NK2 homeobox 2) and *OLIG1* (Oligodendrocyte transcription factor 1); and late regulators, like *MYRF* (Myelin regulatory factor). Regulatory patterns were stage-specific: *MYRF, OLIG1* and *NKX6–2* were differentially expressed at both time points, whereas the 4–5-month group showed broader upregulation, including several additional regulatory genes (e.g., *OLIG2, SOX8* (SRY-box transcription factor 8*), SOX10*), suggesting an increased compensatory demand for myelinating oligodendrocytes. Longitudinal expression (Fig. 2**a**) showed that the myelination peak observed in 3-week-old control pigs was absent in CT pigs at the same age, with catch-up expression by 4–5 months, indicating delayed but compensatory myelination.

Table 2
Biological processes associated with myelin sheath formation and axon ensheathment downregulated in 3-week-old CT pigs and upregulated in 4–5-month-old CT pigs (FDR<0.05).

Downregulated cerebellar genes in 3-week-old CT pigs				
GO term ID	**GO Term name**	**GeneCount**	**FoldEnrich**	**FDR**
GO:0007272	Axon ensheathment	15	15.45	9.2E−10
GO:0008366	Ensheathment of neurons	15	15.45	9.2E−10
GO:0042552	Myelination	14	14.70	8.4E−9
GO:0045685	Regulation of oligodendrocyte differentiation	5	17.50	0.028
GO:00048709	Oligodendrocyte differentiation	6	9.69	0.037
GO:0014003	Oligodendrocyte development	5	14.19	0.037

Upregulated cerebellar genes in 4–5-month-old CT pigs				
GO term ID	**GO Term name**	**GeneCount**	**FoldEnrich**	**FDR**
GO:0008366	Axon ensheathment	21	9.19	2E−10
GO:0007272	Ensheathment of neurons	21	9.19	2E−10
GO:0042552	Myelination	20	8.93	7.6E−10
GO:00048709	Oligodendrocyte differentiation	10	6.87	5.9E−4
GO:0022010	Central nervous system myelination	6	12.75	2.5E−3
GO:0014003	Oligodendrocyte development	7	8.44	4.3E−3

3.4. Modest myelination-related transcriptional changes without significant DEGs in cerebral white matter

In the cerebral white matter, genes encoding myelin proteins showed a clear trend: expression was slightly lower in CT newborn and three-week-olds compared to controls, followed by a modest increase above control levels at 4–5 months (Fig. 2**b**). Genes involved in oligodendrocyte maturation displayed a similar pattern, but with slightly higher expression in CT newborns than controls. However, none of these differences reached statistical significance, and no DEGs associated with myelination or oligodendrocyte development were identified.

3.5. Innate and myeloid immune activation emerges in recovered CT pigs

Among upregulated cerebellar genes in 4–5-month-olds, enriched biological processes included immune activation alongside myelination. While broad immune GO terms (e.g. immune response, inflammatory response) were highly significant (FDR <6.7E−7), they showed lower fold enrichment (<3.2) compared with myelin-related terms. However, pathways related to innate and myeloid immune activity showed higher enrichment, including macrophage activation involved in immune response (11.7), neutrophil activation and neutrophil chemotaxis (9.2 and 6.9), and microglial cell activation involved in immune response (33.5). Positive regulation of myeloid leucocyte mediated immunity was also strongly enriched (12.4), highlighting prominent activation of resident, and potentially infiltrating, myeloid cells.

In the cerebral white matter, no immune activation processes were enriched at 4–5-months. Still, *TLR2* (Toll like receptor 2), a key component of viral detection, was upregulated, mirroring cerebellar upregulation of *TLR2* and *TLR4* (Toll like receptor 4). Both *TLR2* and *TLR4* can respond to Pathogen-Associated Molecular Patters (PAMPs), as well as Damage-Associated Molecular Patterns (DAMPs) derived from tissue injury. RNA-sensing TLRs (TLR3 for dsRNA; TLR7/8 for ssRNA) were not significantly upregulated in either region. Overall, TLR expression trended up with age in CT pigs in both tissues and in the cerebral white matter of controls, whereas controls showed a 3-week peak in cerebellum followed by a decline (Fig. 3**a, b**). This resulted in greater differences in cerebellar TLR expression between 4 and 5-month-old CT pigs and controls compared to cerebral white matter.

Despite progressively higher TLR expression in CT pigs, *IRF3* (Interferon regulatory factor 3), a key transcription factor regulating interferon secretion following TLR activation, remained stable and comparable to controls across ages (Fig. 3**a, b**). Interferon genes (e.g. *IFN-α, IFN-β, IFN-λ, IFN-γ, IFN-κ*) and pro-inflammatory cytokines (e.g. *TNF, IL−1β, IL6, IL12a, IL8*) were consistently low in both groups and both areas at all time points. No elevation of biological processes associated with adaptive immune defence was observed in CT pigs.

3.6. Microglial activity in recovered CT pigs

Although several enriched GO terms in the cerebellum of 4–5-months-old CT pigs supported microglial activation, the specific functional state of these cells was more difficult to determine. Processes associated with phagocytosis, endocytosis, chemotaxis and lipoprotein response were significantly enriched (Supplementary Table S12), indicating an active and mobilised innate immune reaction.

Among microglia-associated DEGs, multiple genes were upregulated in CT cerebellum at 4–5 months. In addition to TLR2 and TLR4, homeostatic markers, such as *TMEM119* (Transmembrane protein 119) and *C1QA* (Complement C1q subcomponent subunit A), as well as activation/repair-associated markers, such as *IBA1* were elevated. Although the TREM2-TYROBP signalling pathway was not enriched at the GO level, both *TREM2* (Triggering receptor expressor expressed on myeloid cells 2) and *TYROBP* (Tyrosine kinase binding protein) were individually upregulated, indicating activation of these receptors without broader pathway engagement. In contrast, key genes involved in lysosomal lipid processing or lipid removal, such as LAMP1 and APOE, were not upregulated, consistent with limited degradation of myelin debris.

Age-dependent increases paralleled TLR trends in both cerebellum and cerebrum, with higher peaks in cerebellum at 4–5 months (Fig. 4**a, b**). Controls again showed a 3-week cerebellar peak not seen in cerebral white matter.

GPNMB (Glycoprotein nonmetastatic melanoma protein B, microglia-enriched, neuroinflammation-linked) showed higher mean expression across all ages in CT pigs in both regions **(**Fig. 4**a, b).** In cerebral white matter it was driven by high intra-group variability: a subset of individuals exhibited markedly elevated expression, while others resembled controls. In contrast, *LOC100520753,* corresponding to a CD68 transcript variant linked to microglial activity, showed consistently higher expression in CT individuals across ages in both cerebral white matter and cerebellum, although overall expression levels remained low (Fig. 4**c, d**).

3.7. KEGG pathway enrichment supports innate immune activation in cerebellum

KEGG analysis of upregulated DEGs in pooled cerebellar samples from recovered CT pigs identified 17 pathways, complementing the functional enrichment results at the pathway level (Supplementary Table S14). Several pathways supported innate immune activation, including Complement and Coagulation cascades, Phagosome, Phospholipase D signalling pathway and the Toll-like receptor signalling pathway**.** Additional immune-related pathways were mapped to KEGG modules associated with specific viral or bacterial infections, reflecting broader activation of pattern-recognition and inflammatory signalling rather than pathogen-specific responses. Beyond immune pathways, KEGG analysis also revealed enrichment of processes related to lipid metabolism and cell adhesion molecules.

Among upregulated cerebellar genes in 3-week-old CT pigs, a single KEGG pathway was enriched, corresponding to Protein digestion and absorption (Supplementary Table S15).

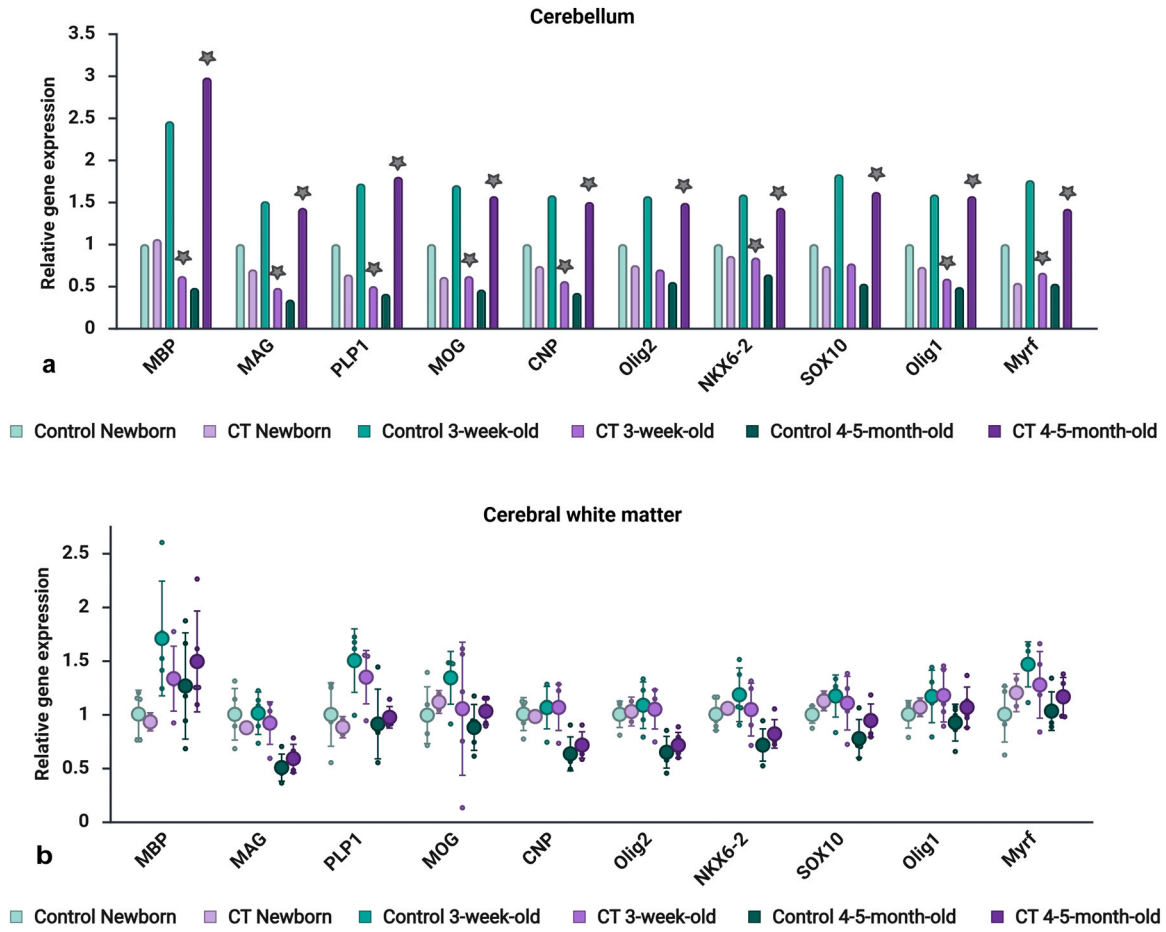

Fig. 2. Longitudinal relative expression of key genes involved in myelination and oligodendrocyte differentiation. Statistically significant differences (FDR <0.05) are indicated by stars. **(a)** Cerebellum: controls showed a peak at three weeks followed by a decline at 4–5 months, whereas CT pigs lacked the 3-week peak but exhibited a compensatory increase at 4–5 months. **(b)** Cerebral white matter: no significant differences were detected, though CT pigs trended lower than controls at three weeks and slightly higher at 4–5 months. Data is shown as mean (large circles) ± SD (whiskers), with individual samples represented by smaller points.

3.8. Astrocyte markers track with myelination-related genes

In the cerebellum, astrocyte-related processes (e.g. development, differentiation) were enriched (FDR < 0.05) in 4–5-month-old CT pigs, alongside upregulation of *GFAP* and *S100B* (S100 calcium binding protein B) (Supplementary Table S16**)**. At 3-weeks, CT expression of these markers was lower than controls, mirroring many myelination genes. No significant astrocyte-specific differences were detected in the cerebral white matter.

3.9. Immunohistochemistry confirms glial alteration and mild myelin pathology

Glial markers were selected based on enhanced cerebellar gene expression in 4–5-month-old CT pigs: GFAP (astrocytes), IBA1 (microglia and macrophages), OLIG2 (oligodendrocytes) and MBP (myelin and myelinating oligodendrocytes). Detailed description of cerebellar RNA-seq results for glial markers are provided in Supplementary Table S16**.**

3.10. Astrocytes: Increased GFAP in newborn CT pigs

Newborn CT pigs showed a significantly higher GFAP + area compared to controls (CT: mean = 20.4%, SD= 4.13, 95% CI= 15.3–25.5; Control: mean =11.0%, SD=2.81, 95% CI=7.54–14.5 (Fig. 5**a-c**). Astrocyte numbers appeared similar, but CT pigs exhibited diffuse hypertrophy, and greater 1 + and 2 + staining intensity. No differences were observed in older groups.

3.11. Microglia: Increased microaggregates during recovery

IBA + area within the four lateral ROIs showed no significant difference. However, when counted in a larger area, CT pigs had significantly more microglial microaggregates in unbranched white matter at 3 weeks and 4–5 months, with the largest increase in the oldest group (CT: mean = 25.2 microaggregates, SD= 17.9, 95% CI= 3.0–47.4; Control: mean = 3.4 microaggregates, SD= 3.21, 95% CI= −0.6–7.4) (Fig. 5**d-f**). Aggregates were multifocal, and the microglia displayed a ramified rather than highly amoeboid appearance, explaining why IBA + area did not differ for the smaller region of interest.

3.12. Oligodendrocytes and myelin: Minimal differences

OLIG2 + cell density decreased with age in both groups, with no significant differences between CT pigs and controls. A trend toward fewer strongly stained OLIG2 + cells (3 +) was noted in 3-week-old CT pigs (p = 0.15).

MBP analysis revealed a small but significant reduction in MBP + area in CT newborns (p = 0.016), but no differences in older groups (Fig. 5**g**). Variability in MBP + area in newborn and 3-week-old CT pigs reflected focal regions of myelin vacuoles of various size, absent in controls and largely resolved by 4–5 months (Fig. 5**h, i**), as documented previously (Bergfeldt et al., 2025).

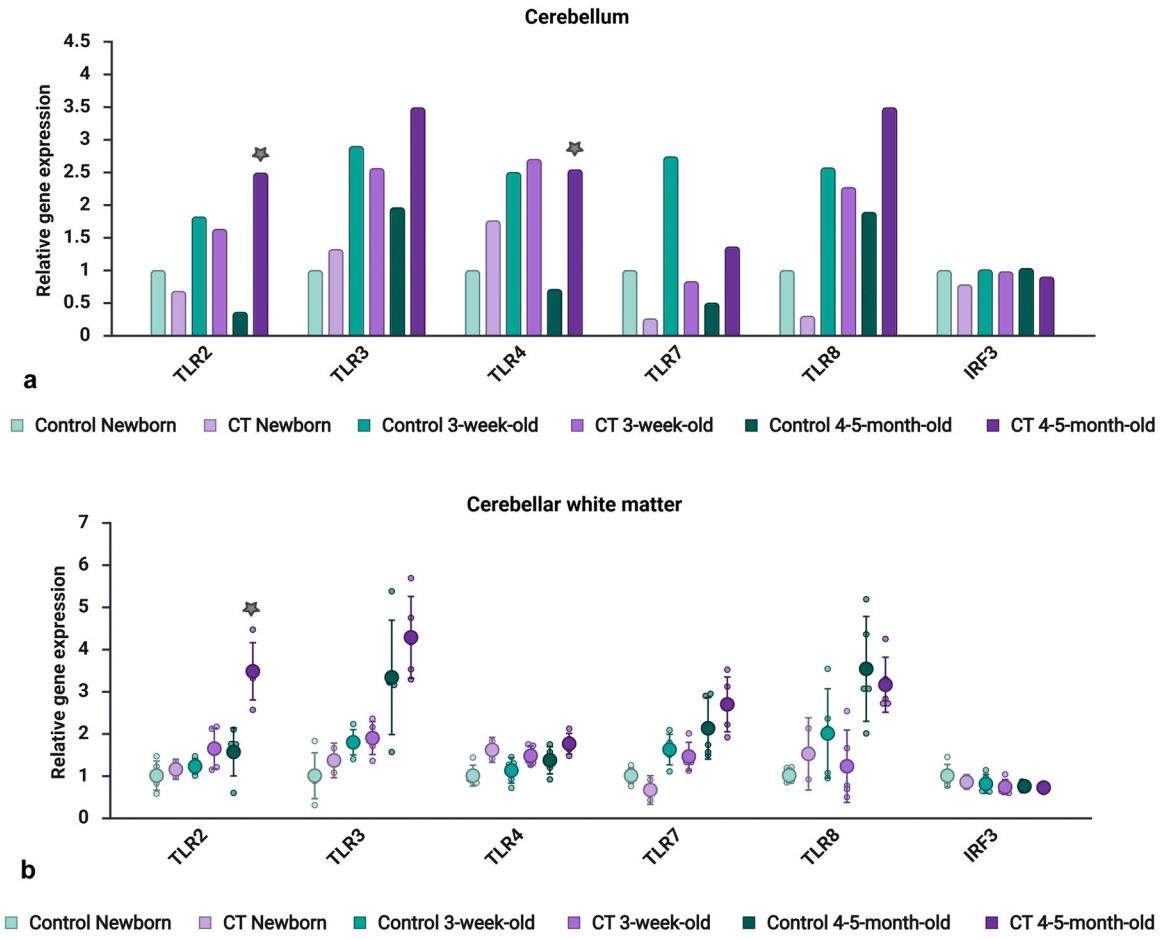

Fig. 3. Longitudinal expression of genes associated with interferon signalling, antiviral response and viral recognition. Statistically significant differences (FDR <0.05) are indicated by stars. **(a)** Expression of *TLR* (Toll like receptor) genes and *IRF3* (Interferon regulatory factor 3) in pooled cerebellar samples from CT pigs and controls across newborn, 3-week-old, and 4–5 months. **(b)** Expression of the same *TLR* genes and *IRF3* in individual cerebral white matter samples. Data is shown as mean (large circles) ± SD (whiskers), with individual samples represented by smaller points.

4. Discussion

Congenital tremor type A-II, caused by *in utero* infection with APPV, results in involuntary tremors that typically resolve with age despite prolonged viral presence in the CNS. This raises questions about APPV's impact on postnatal CNS development and its ability to persist without effective clearance. To address this, we conducted a longitudinal case-control study of pigs recovering from severe CT A-II, combining cerebellar and cerebral white matter transcriptomics at different levels of resolution with immunohistochemistry to investigate APPV pathogenesis, recovery mechanisms, and virus-host immune interactions.

In pigs, myelination peaks before birth and again around three weeks postnatally (Sweasey et al., 1976). Controls reflected this pattern, showing a clear peak in myelination-related gene expression at three weeks, higher in the cerebellum than cerebral white matter, followed by a decline at 4–5 months. CT pigs deviated markedly: at three weeks, myelination genes were expressed lower than controls, but at 4–5 months, levels exceeded controls, suggesting delayed and prolonged myelination (Fig. 2**a**). This delay was most pronounced in the cerebellum, consistent with previous documentation of transient cerebellar hypomyelination (Bergfeldt et al., 2025). Cerebral white matter changes were milder but followed similar trends (Fig. 2**b**). Greater cerebellar impact likely reflects APPV's tropism and higher viral loads in this region (Postel et al., 2016; Liu et al., 2019; Bergfeldt et al., 2025). Combined with reports of spinal cord hypomyelination (Schwarz et al., 2017; Dessureault et al., 2018), our findings suggest a widespread, though variable, disruptive effect of APPV on CNS myelination, with spinal cord and cerebellum most affected. However, the *in utero* mechanisms driving hypomyelination remain unclear, and these processes may affect different CNS regions to varying degrees.

Despite significant transcriptional differences, IHC for MBP showed no marked group differences (Fig. 5**g**). Absence of obvious myelin loss supports mild hypomyelination as a CT A-II feature (Schwarz et al., 2017; Stenberg et al., 2022; Bergfeldt et al., 2025), possibly also explained by slow MBP turnover and compact hypomyelinated sheaths retaining normal MBP levels (Toyama et al., 2013; Bagheri et al., 2024). OLIG2 + cell density was similar across groups, suggesting hypomyelination stems from delayed oligodendrocyte maturation rather than reduced numbers, aligning with previous CT studies (Schwarz et al., 2017). Mechanisms may involve transient prenatal damage to oligodendrocyte precursors, as seen in BVDV infections (Bielefeldt-Ohmann et al., 2012), followed by compensatory proliferation and maturation arrest (Segovia et al., 2008). Future work should assess oligodendrocyte linage composition using markers for immature oligodendrocytes (e.g., O4).

Among pestiviruses, border disease virus (BDV) provides the most relevant comparison to APPV-associated hypomyelination, as prenatal BDV infection can result in congenital tremor and hypomyelination, with progressive clinical recovery and partial normalization of myelin when the initial injury is not severe (Barlow and Dickinson, 1965). In comparison, APPV-associated hypomyelination appears milder and is associated with a more rapid recovery.

The surrounding microenvironment, including microglial and astrocytic activity, also regulates oligodendrocyte development

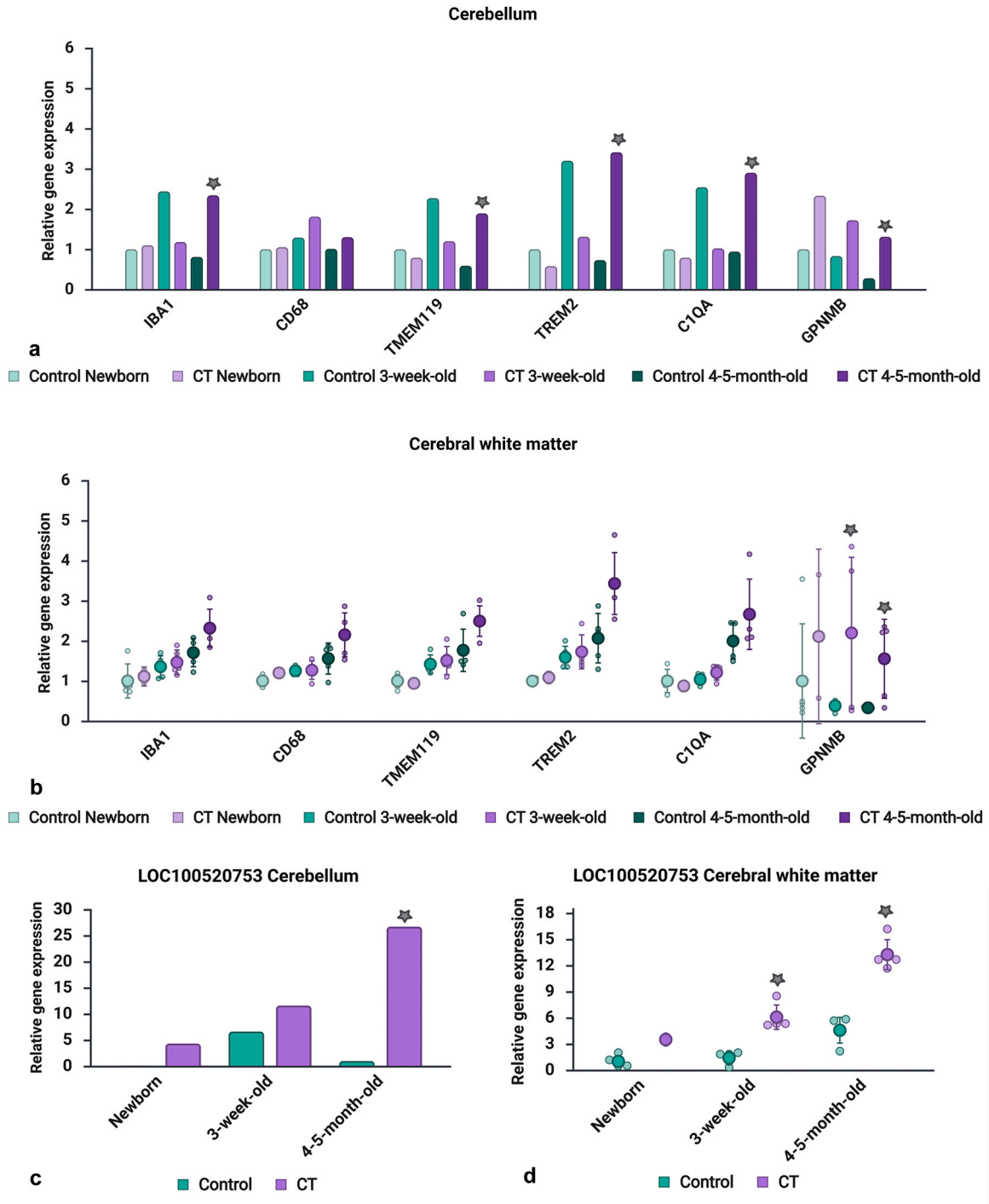

Fig. 4. Longitudinal gene expression of genes associated with different microglial states in CT pigs and controls. Statistically significant differences in gene expression (DEG) are indicated by stars (FDR <0.05). (**a**) Gene expression of selected microglia-associated genes in the cerebellum. (**b**) Gene expression of the same microglia-associated genes in the cerebral white matter. Data is shown as mean (large circles) ± SD (whiskers), with individual samples represented by smaller points. **(c-d)** Longitudinal expression of LOC100520753 (microglia-linked) in cerebellar pooled samples (c) and individual cerebral white matter samples (d).

(Traiffort et al., 2020). While RNA-seq revealed no upregulation of astrocyte transcripts in CT newborns in the present study, IHC demonstrated a diffuse increase in hypertrophic GFAP + astrocytes (Fig. 5**a**), indicating hypertrophic astrogliosis (Zamanian et al., 2012). This response, undetected by routine histology, may contribute to impaired oligodendrocyte maturation (Segovia et al., 2008). The absence of GFAP transcript elevation may reflect protein stability (Rolland et al., 1990), possibly persisting from a prenatal increase in astrocyte activity. The discrepance from previous reports of more severe astrogliosis in CT newborns (Possatti et al., 2018) may reflect methodological differences, atypical cases or co-infection.

Pestiviruses evade innate immunity via two interferon-antagonists: E^{rns} and N^{pro}. E^{rns} acts as an unspecific RNase, while N^{pro} inhibits interferon induction by supressing IRF3 post-translationally and targeting the IRF3 protein for proteasomal degradation (Seago et al., 2007; Peterhans and Schweizer, 2010). Our finding that IRF3 gene expression remained stable during prolonged APPV infection (Fig. 3**a, b**) is consistent with earlier in vitro studies (Bauhofer et al., 2007) showing

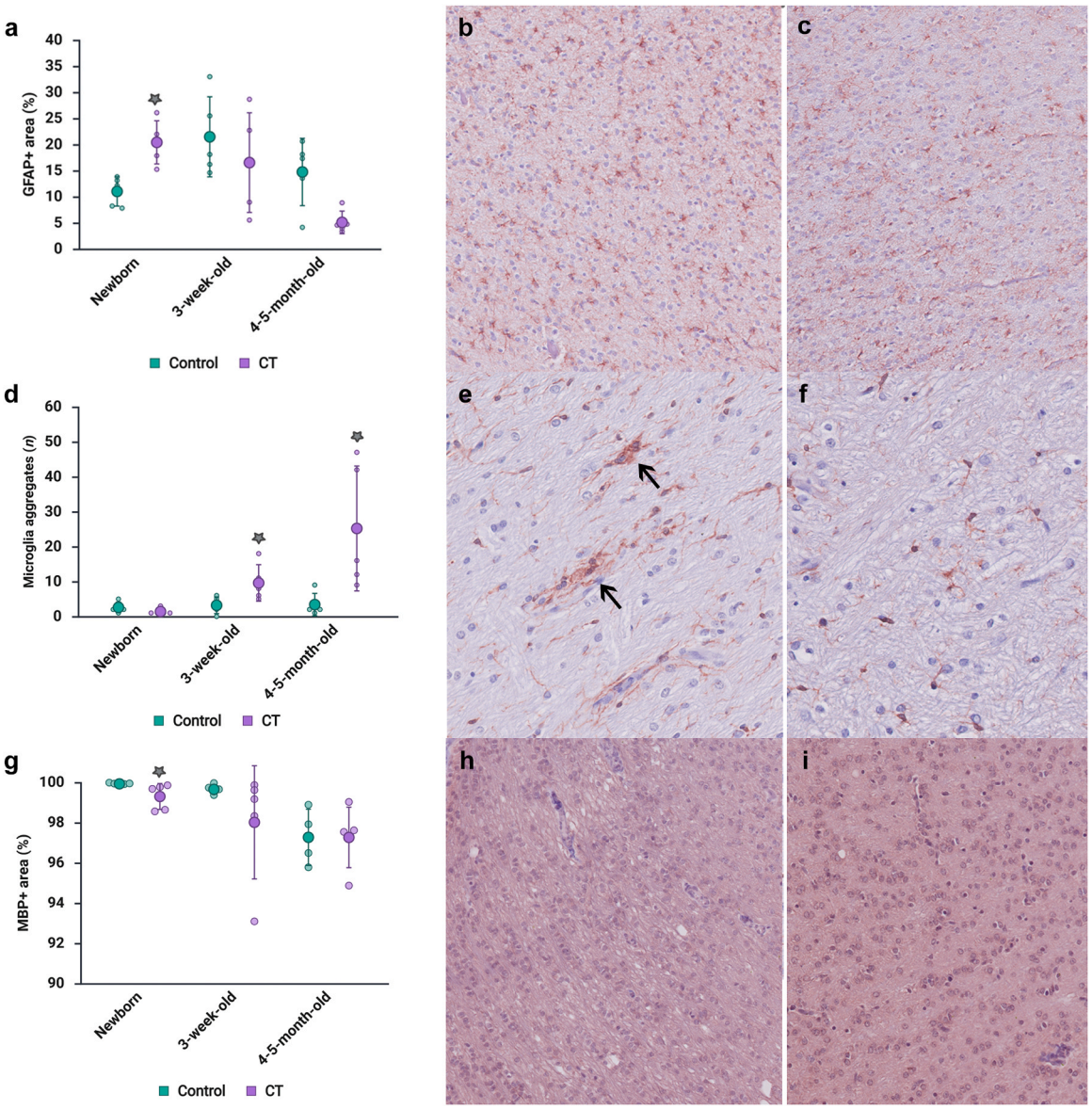

Fig. 5. Cerebellar immunohistochemistry for glial and myelin markers in CT pigs and controls across age groups. **(a-c)** GFAP immunolabeling newborn CT pigs showed a significantly larger area of GFAP + area compared to controls (a), with diffuse astrocyte hypertrophy rather than focal aggregates (b), whereas control newborn exhibited smaller GFAP + areas (c). **(d-f)** IBA1 immunolabeling: CT pigs displayed a significant increase in multifocal microglial aggregates in white matter at 3 weeks and 4–5 months (d), illustrated by clusters of IBA1 + cells in CT pigs (e), and their relative absence in controls (f). **(g-i)** MBP immunolabeling: MBP-positive area was slightly reduced in CT newborns (g), with focal myelin vacuoles of various size in newborn and 3-week-old CT pigs (h), absent in controls (i).

that pestiviral N^{pro} mediates IRF3 degradation without altering IRF3-mRNA levels. Nevertheless, the absence of interferon-related gene activation, despite viral persistence and progressively higher TLR expression in CT pigs, suggests ongoing activity of one or both viral interferon antagonist (E^{rns} and N^{pro}). Although *STING* (Stimulator of Interferon Genes) upregulation has been reported in CT newborns (Stenberg et al., 2022), it was not found here, possibly due to low baseline expression or subtle changes.

Recovered CT pigs showed microglial activation. RNA-seq revealed age-dependent increases in microglia-related genes (Fig. 4**a, b**), especially in the cerebellum, supported by IHC showing focal microglial aggregates with ramified morphology (Fig. 5**b**), indicative of surveillance and repair rather than robust phagocytosis (Schafer et al., 2012). Upregulation of *TREM2*, *TYROBP* and complement genes suggests recognition and opsonisation, while the more moderate increase in phagocytic markers (e.g. *LAMP1, APOE*) indicates limited phagocytic activity. Persistent APPV RNA or residual myelin debris may drive this response. Microglial activation likely reflects ongoing low-grade antigenic stimulation or delayed clearance of myelin debris.

Despite these findings, interpretation of microglia-related results was complicated by regional differences. Expression patterns in controls differed between cerebellum and cerebrum: cerebral white matter showed a progressive age-related increase, whereas cerebellum exhibited a transient peak at three weeks. Microglia are known to regulate myelin growth during CNS development, preventing hypermyelination (McNamara et al., 2024). These differences may reflect a developmental regulatory phase in the cerebellum that does not temporally overlap with that in the cerebrum. Differences in microglial density between grey and white matter may also have contributed to the observed regional variation, as the cerebellar samples represented a mixture of both compartments, whereas the cerebral samples consisted predominantly of white matter. However, this sampling difference does not explain the consistently higher microglial gene expression in CT pigs compared to controls in cerebral white matter, supporting the

conclusion of a more widespread microglial activation in the CNS.

Notably, *GPNMB* and *LOC100520753*, showed elevated expression in both areas across all CT age groups (Fig. 4**a-d**), marking them as candidates for further study. *GPNMB*, a transmembrane glycoprotein upregulated in disease-associated microglia (Huttenrauch et al., 2018), is often linked to anti-inflammatory rather than pro-inflammatory responses (Saade et al., 2021). Here, *GPNMB* was upregulated in some CT individuals, primarily those with the lowest degree of white matter vacuolization, suggesting a heterogenous microglial response. *LOC100520753* represents a CD68 transcript variant (NCBI, 2026). Their co-expression suggests overlapping roles in macrophage/microglia-linked functions (Hase et al., 2022), and despite low overall expression, the consistent CT-linked increase of LOC100520753 may indicate mild but stable microglial activation. However, given the observed inter-individual variability and low absolute expression levels, these findings should be interpreted as hypothesis-generating rather than evidence of robust biomarker potential.

A limitation of the present study is the use of pooled RNA samples for cerebellar transcriptomic analysis. While pooling enabled identification of robust, group-level transcriptional patterns associated with APPV infection and recovery, it precluded assessment of inter-individual variability and limited sensitivity for detecting subtle or heterogeneous gene expression changes. Accordingly, cerebellar RNA-seq findings reflect consistent group-level trends rather than individual expression profiles. Importantly, the main biological interpretations are supported by convergent evidence from complementary methodologies, including immunohistochemistry, ultrastructural analysis, and individual-level RNA-seq of cerebral white matter. Taken together, these data support the interpretation of delayed and prolonged myelination as a group characteristic of CT A-II recovery.

Future approaches, including IHC for markers of phagocytic or antigen-presenting microglial phenotypes, in situ viral RNA mapping to determine the cellular and spatial localization of APPV within the CNS, and single-cell RNA-seq, could further clarify microglial functional states and host-virus interactions in CT A-II. In addition, studies targeting protein expression and activation of key interferon pathway components, such as IRF3 phosphorylation and interferon activity, will be required to directly confirm interferon antagonistic mechanisms of APPV in vivo. Together, such approaches would help resolve the relationship between viral persistence, regional host response and functional recovery in the CNS.

5. Conclusions

This study characterised cerebral and cerebellar processes affected by APPV during clinical disease and recovery from CT A-II, integrating transcriptomics and immunohistochemistry. APPV likely disrupted oligodendrocyte maturation and myelin production during critical developmental periods, causing delayed myelination across the CNS, more pronounced in cerebellum. Despite this, preserved oligodendrocyte populations and later upregulation of myelination-related genes in recovered pigs demonstrate the CNS's capacity for delayed repair.

The absence of overt inflammation early in disease highlights APPV's immunosuppressive potential, consistent with pestivirus immunomodulation. However, astrocyte hypertrophy in newborns and microglial aggregates in recovered pigs indicate dynamic glial involvement in remodelling and antigen recognition. Correlating these findings with transcriptomic profiles underscores astrocyte and microglial roles in myelin recovery.

Altogether, this work provides new insights into APPV pathogenesis and recovery, emphasising glial plasticity as a key factor in the response to APPV-induced myelination delay.

Author contributions

Conceptualisation, A.B., M. A.T., R.S.; formal analysis, A.B.; investigation, A.B.; writing—original draft preparation, A.B.; writing—review and editing, A.B., M. A.T., and R.S.; visualisation, A.B.; supervision, M. A.T., and R.S. All authors have read and agreed to the published version of the manuscript.

CRediT authorship contribution statement

Michael A. Tranulis: Writing – review & editing, Supervision, Conceptualization. **Anna Bergfeldt:** Writing – review & editing, Writing – original draft, Visualization, Investigation, Funding acquisition, Formal analysis, Conceptualization. **Randi Sørby:** Writing – review & editing, Supervision, Conceptualization.

Declaration of Generative AI and AI-assisted technologies in the writing process

During the preparation of this work, the authors used Microsoft Copilot to assist with improving sentence structure, clarity and overall readability of the manuscript. After using this tool, the authors reviewed and edited the content as needed and take full responsibility for the final version of the manuscript.

Funding

This research has received funding from the Faculty of Veterinary medicine at the Norwegian University of Life Sciences (project number 1351025105), with contributions from Astri and Birger Torsted Foundation.

Declaration of Competing Interest

The authors declare that they have no known competing financial interests or personal relationships that could have appeared to influence the work reported in this paper.

Acknowledgements

We thank Dr. Rasoul Nourizadeh-Lillabadi for assistance with laboratory work, and Dr. Erik Rasmussen for fruitful discussions concerning the transcriptome analyses. We are especially grateful to the pig producers who participated in this study. Their contribution was essential to making this research possible.

Appendix A. Supporting information

Supplementary data associated with this article can be found in the online version at doi:10.1016/j.vetmic.2026.111095.

References

Aae, F.H., Stokstad, M., Myrmel, M., Sørby, R., Bergfeldt, A., Ranheim, B., 2025. Tremor tales: a cohort study of general and neurological signs in pigs with atypical porcine pestivirus-induced congenital tremor. Vet. J. 309, 106288.

Arruda, B.L., Arruda, P.H., Magstadt, D.R., Schwartz, K.J., Dohlman, T., Schleining, J.A., et al., 2016. Identification of a divergent lineage porcine pestivirus in nursing piglets with congenital tremors and reproduction of disease following experimental inoculation. PLoS One 11 (2), e0150104.

Bagheri, H., Friedman, H., Hadwen, A., Jarweh, C., Cooper, E., Oprea, L., et al., 2024. Myelin basic protein mRNA levels affect myelin sheath dimensions, architecture, plasticity, and density of resident glial cells. Glia 72 (10), 1893–1914.

Bankhead, P., Loughrey, M.B., Fernandez, J.A., Dombrowski, Y., McArt, D.G., Dunne, P. D., et al., 2017. QuPath: Open source software for digital pathology image analysis. Sci. Rep. 7 (1), 16878.

Barlow, R.M., Dickinson, A.G., 1965. On the pathology and histochemistry of the central nervous system in border disease of sheep. Res. Vet. Sci. 6, 230–237.

Bauhofer, O., Summerfield, A., Sakoda, Y., Tratschin, J.D., Hofmann, M.A., Ruggli, N., 2007. Classical swine fever virus Npro interacts with interferon regulatory factor 3 and induces its proteasomal degradation. J. Virol. 81 (7), 3087–3096.
Bergfeldt, A., Myrmel, M., Ranheim, B., Aae, F., Sorby, R., 2025. Cerebellar hypomyelination, white matter vacuolization, and prolonged presence of atypical porcine pestivirus in pigs with congenital tremor type A-II. Vet. Pathol. 3009858251372559.
Bielefeldt-Ohmann, H., Smirnova, N.P., Tolnay, A.E., Webb, B.T., Antoniazzi, A.Q., van Campen, H., et al., 2012. Neuro-invasion by a 'Trojan Horse' strategy and vasculopathy during intrauterine flavivirus infection. Int. J. Exp. Pathol. 93 (1), 24–33.
Buckley, A.C., Falkenberg, S.M., Palmer, M.V., Arruda, P.H., Magstadt, D.R., Schwartz, K. J., et al., 2021. Distribution and persistence of atypical porcine pestivirus in experimentally inoculated pigs. J. Vet. Diagn. Invest. 33 (5), 952–955.
Cagatay, G.N., Meyer, D., Wendt, M., Becher, P., Postel, A., 2019. Characterization of the humoral immune response induced after infection with atypical porcine pestivirus (APPV). Viruses 11 (10).
Dall Agnol, A.M., Alfieri, A.F., Alfieri, A.A., 2020. Pestivirus K (atypical porcine pestivirus): update on the virus, viral infection, and the association with congenital tremor in newborn piglets. Viruses 12 (8).
Dessureault, F.G., Choinière, M., Provost, C., Gagnon, C.A., 2018. First report of atypical porcine pestivirus in piglets with congenital tremor in Canada. Can. Vet. J. 59 (4), 429–432.
Felix, B., Leger, M.E., Albe-Fessard, D., Marcilloux, J.C., Rampin, O., Laplace, J.P., 1999. Stereotaxic atlas of the pig brain. Brain Res. Bull. 49 (1-2), 1–137.
de Groof, A., Deijs, M., Guelen, L., van Grinsven, L., van Os-Galdos, L., Vogels, W., et al., 2016. Atypical porcine pestivirus: a possible cause of congenital tremor type A-II in newborn piglets. Viruses 8 (10).
Hase, Y., Ameen-Ali, K.E., Waller, R., Simpson, J.E., Stafford, C., Mahesh, A., et al., 2022. Differential perivascular microglial activation in the deep white matter in vascular dementia developed post-stroke. Brain Pathol. 32 (6), e13101.
Hause, B.M., Collin, E.A., Peddireddi, L., Yuan, F., Chen, Z., Hesse, R.A., et al., 2015. Discovery of a novel putative atypical porcine pestivirus in pigs in the USA. J. Gen. Virol. 96 (10), 2994–2998.
Huttenrauch, M., Ogorek, I., Klafki, H., Otto, M., Stadelmann, C., Weggen, S., et al., 2018. Glycoprotein NMB: a novel Alzheimer's disease associated marker expressed in a subset of activated microglia. Acta Neuropathol. Commun. 6 (1), 108.
Liu, J., Li, Z., Ren, X., Li, H., Lu, R., Zhang, Y., et al., 2019. Viral load and histological distribution of atypical porcine pestivirus in different tissues of naturally infected piglets. Arch. Virol. 164 (10), 2519–2523.
McNamara, N.B., Munro, D.A.D., Bestard-Cuche, N., Uyeda, A., Bogie, J.F.J., Hoffmann, A., et al., 2024. Author Correction: Microglia regulate central nervous system myelin growth and integrity. Nature 631 (8021), E11.
National Center for Biotechnology Information (NCBI), 2026. Gene: LOC100520753 [Internet]. Available from: https://www.ncbi.nlm.nih.gov/gene/?term=LOC100520753.
Peterhans, E., Schweizer, M., 2010. Pestiviruses: how to outmaneuver your hosts. Vet. Microbiol. 142 (1-2), 18–25.
Possatti, F., de Oliveira, T.E.S., Leme, R.A., Zotti, E., Dall Agnol, A.M., Alfieri, A.F., et al., 2018. Pathologic and molecular findings associated with atypical porcine pestivirus infection in newborn piglets. Vet. Microbiol. 227, 41–44.
Postel, A., Hansmann, F., Baechlein, C., Fischer, N., Alawi, M., Grundhoff, A., et al., 2016. Presence of atypical porcine pestivirus (APPV) genomes in newborn piglets correlates with congenital tremor. Sci. Rep. 6, 27735.
Rolland, B., Le Prince, G., Fages, C., Nunez, J., Tardy, M., 1990. GFAP turnover during astroglial proliferation and differentiation. Brain Res. Dev. Brain Res. 56 (1), 144–149.
Saade, M., Araujo de Souza, G., Scavone, C., Kinoshita, P.F., 2021. The Role of GPNMB in Inflammation. Front. Immunol. 12, 674739.
Schafer, D.P., Lehrman, E.K., Kautzman, A.G., Koyama, R., Mardinly, A.R., Yamasaki, R., et al., 2012. Microglia sculpt postnatal neural circuits in an activity and complement-dependent manner. Neuron 74 (4), 691–705.
Schwarz, L., Riedel, C., Hogler, S., Sinn, L.J., Voglmayr, T., Wochtl, B., et al., 2017. Congenital infection with atypical porcine pestivirus (APPV) is associated with disease and viral persistence. Vet. Res. 48 (1), 1.
Seago, J., Hilton, L., Reid, E., Doceul, V., Jeyatheesan, J., Moganeradj, K., et al., 2007. The Npro product of classical swine fever virus and bovine viral diarrhea virus uses a conserved mechanism to target interferon regulatory factor-3. J. Gen. Virol. 88 (Pt 11), 3002–3006.
Segovia, K.N., McClure, M., Moravec, M., Luo, N.L., Wan, Y., Gong, X., et al., 2008. Arrested oligodendrocyte lineage maturation in chronic perinatal white matter injury. Ann. Neurol. 63 (4), 520–530.
Stenberg, H., Hellman, S., Lindstrom, L., Jacobson, M., Fossum, C., Hayer, J., et al., 2022. Congenital tremor and splay leg in piglets - insights into the virome, local cytokine response, and histology. BMC Vet. Res. 18 (1), 348.
Stenberg, H., Jacobson, M., Malmberg, M., 2020. A review of congenital tremor type A-II in piglets. Anim. Health Res. Rev. 21 (1), 84–88.
Sweasey, D., Patterson, D.S., Glancy, E.M., 1976. Biphasic myelination and the fatty acid composition of cerebrosides and cholesterol esters in the developing central nervous system of the domestic pig. J. Neurochem. 27 (2), 375–380.
Toyama, B.H., Savas, J.N., Park, S.K., Harris, M.S., Ingolia, N.T., Yates, J.R., 3rd, et al., 2013. Identification of long-lived proteins reveals exceptional stability of essential cellular structures. Cell 154 (5), 971–982.
Traiffort, E., Kassoussi, A., Zahaf, A., Laouarem, Y., 2020. Astrocytes and microglia as major players of myelin production in normal and pathological conditions. Front. Cell. Neurosci. 14, 79.
Zamanian, J.L., Xu, L., Foo, L.C., Nouri, N., Zhou, L., Giffard, R.G., et al., 2012. Genomic analysis of reactive astrogliosis. J. Neurosci. 32 (18), 6391–6410.

Glossary

AEC: 3-Amino-9-ethylcarbazole (chromogen for IHC)
APOE: Apolipoprotein E
APPV: Atypical Porcine Pestivirus
bp: Base Pair
BP: Biological Process
cDNA: Complementary DNA
CD68: Cluster of Differentiation 68
CI: Confidence Interval
C1qA: Complement C1q subcomponent subunit A
CNP: 2′,3′-Cyclic-Nucleotide 3′-Phosphodiesterase
CNS: Central Nervous System
CT: Congenital Tremor
DAB: 3,3′-Diaminobenzidine (chromogen for IHC)
DAMP: Damage-Associated Molecular Pattern
DAVID: Database for Annotation, Visualization and Integrated Discovery
DEGs: Differentially Expressed Genes
dsRNA: Double-Stranded RNA
dUTP: Deoxyuridine Triphosphate
EDTA: Ethylenediaminetetraacetic Acid
E^{rns}: Envelope RNase (pestivirus protein)
FASTQ: FASTQ File Format (for sequencing reads)
FDR: False Discovery Rate
FoldEnrich: Fold Enrichment
FPKM: Fragments Per Kilobase of transcript per Million mapped reads
GC: Guanine-Cytosine content
GFAP: Glial Fibrillary Acidic Protein
GO: Gene Ontology
GPNMB: Glycoprotein Non-Metastatic Melanoma Protein B
h: Hour
HRP: Horseradish Peroxidase
H-score: Histological Score
IBA1: Ionized Calcium-Binding Adapter Molecule 1
ID: Identifier
IFN: Interferon
IL: Interleukin
IHC: Immunohistochemistry
IRF3: Interferon Regulatory Factor 3
KEGG: Kyoto Encyclopedia of Genes and Genomes
LAMP: Lysosomal-Associated Membrane Protein
MAG: Myelin-Associated Glycoprotein
MAL: Myelin and Lymphocyte Protein
MBP: Myelin Basic Protein
min: Minute
mm^2: Square Millimeter
mRNA: Messenger RNA
MYRF: Myelin Regulatory Factor
N^{pro}: N-terminal Protease (pestivirus protein)
NKX6-2: NK2 Homeobox 2
OLIG1: Oligodendrocyte Transcription Factor 1
OLIG2: Oligodendrocyte Transcription Factor 2
PAMP: Pathogen-Associated Molecular Pattern
PBS: Phosphate-Buffered Saline
PCR: Polymerase Chain Reaction
PLP1: Proteolipid Protein 1
pH: Potential of Hydrogen
qPCR: Quantitative Polymerase Chain Reaction
Q30: Quality Score 30 (sequencing metric)
RNA: Ribonucleic Acid
RNA-seq: RNA Sequencing
RIN: RNA Integrity Number
ROI: Region of Interest
S100B: S100 Calcium-Binding Protein B
SD: Standard Deviation
SOX8: SRY-Box Transcription Factor 8
SOX10: SRY-Box Transcription Factor 10
ssRNA: Single-Stranded RNA
STING: Stimulator of Interferon Genes
TBS: Tris-Buffered Saline
TIFF: Tagged Image File Format
TLR: Toll-Like Receptor
TMEM119: Transmembrane Protein 119
TREM2: Triggering Receptor Expressed on Myeloid Cells 2
TYROBP: Tyrosine kinase binding protein
μm: Micrometer